Biosynthesis of Copper Nanoparticles Using Hylocereus costaricensis Peel Extract and their Photocatalytic Properties

Suriati Eka Putri
Department of Chemistry, Faculty of Mathematics and Natural Science, Universitas Negeri Makassar, South Sulawesi, Indonesia, ekaputri_chem@unm.ac.id

Netti Herawati
Department of Chemistry, Faculty of Mathematics and Natural Science, Universitas Negeri Makassar, South Sulawesi, Indonesia

Ahmad Fudhail
Department of Chemistry, Faculty of Mathematics and Natural Science, Universitas Negeri Makassar, South Sulawesi, Indonesia

Diana Eka Pratiwi
Department of Chemistry, Faculty of Mathematics and Natural Science, Universitas Negeri Makassar, South Sulawesi, Indonesia

Sumiati Side
Department of Chemistry, Faculty of Mathematics and Natural Science, Universitas Negeri Makassar, South Sulawesi, Indonesia

See next page for additional authors

University of **Kerbala**

Biosynthesis of Copper Nanoparticles Using Hylocereus costaricensis Peel Extract and their Photocatalytic Properties

Abstract

A green chemistry method was used for the first time to synthesize copper nanoparticles (Cu-NPs) using CuSO4 as a precursor and red dragon fruit (Hylocereus costaricensis) peel wasted extract as a bio-reductor. Cu-NPs produced were then used as a photocatalysts for acid orange 7 (AO7) dyes degradation. The results showed that the smallest average crystallite size of the products ranged from 8.84 - 8.86 nm, and the FCC crystal structure had a surface area of 244.38-278.85 m2g-1. Furthermore, the optimum degradation of AO7 dye occurred at a ratio of 1:3 with a percentage of 81.07% for four cycles. These findings indicated that Cu-NPs can be used for the treatment of textile wastewater under sunlight in the future.

Keywords

Copper nanoparticles; bioreduction; red dragon fruit; acid orange

Creative Commons License

Cover Page Footnote

Authors

Suriati Eka Putri, Netti Herawati, Ahmad Fudhail, Diana Eka Pratiwi, Sumiati Side, Abd Rahman, Susilo Sudarman Desa, Nur Ahmad, Subaer Junaedi, and A. Surleva

Biosynthesis of Copper Nanoparticles Using *Hylocereus Costaricensis* Peel Extract and its Photocatalytic Properties

Suriati E. Putri [a],*, Netti Herawati [a], Ahmad Fudhail [a], Diana E. Pratiwi [a], Sumiati Side [a], Abd Rahman [b], Susilo S. Desa [c], Nur Ahmad [d], Subaer Junaedi [e], A. Surleva [f]

[a] Department of Chemistry, Faculty of Mathematics and Natural Science, Universitas Negeri Makassar, Makassar, South Sulawesi, Indonesia
[b] Inorganic Chemistry, King Fahd University of Petroleum & Minerals, Dhahran, Saudi Arabia
[c] School of Bio-Chemical Engineering and Technology, Sirindhorn International Institute of Technology, Thammasat University, Pathum Thani, Thailand
[d] Graduate School, Faculty of Mathematics and Natural Sciences, Sriwijaya University, South Sumatera, Indonesia
[e] Department of Physics, Faculty of Mathematics and Natural Science, Universitas Negeri Makassar, South Sulawesi, Indonesia
[f] Analytical Chemistry Department, University of Chemical Technology and Metallurgy, Sofia, Bulgaria

Abstract

A green chemistry method was used for the first time to synthesize copper nanoparticles (Cu-NPs) using $CuSO_4$ as a precursor and red dragon fruit (*Hylocereus costaricensis*) peel wasted extract as a bio-reductor. Cu-NPs produced were then used as a photocatalysts for acid orange 7 (AO7) dyes degradation. The results showed that the smallest average crystallite size of the products ranged from 8.84 to 8.86 nm with the FCC crystal structure and surface area of $244.38-278.85$ $m^2 g^{-1}$. Furthermore, the optimum degradation of AO7 dye occurred at a ratio of 1:3 with a percentage of 81.07% for four cycles. These findings indicated that Cu-NPs can be used for the treatment of textile wastewater under sunlight in the future.

Keywords: Copper nanoparticles, Bioreduction, Red dragon fruit, Acid orange

1. Introduction

Nanotechnology is a new scientific revolution with enormous potential in several industries. Furthermore, copper nanoparticles (Cu-NPs) are one of the metallic nanomaterials that have received considerable attention. This is due to their unique physical and chemical properties [1], such as the large surface area to volume ratio and size-dependent reactivity, which make them usable as adsorbents and catalysts. In further studies, the application of these materials has been intensively discussed, such as antioxidant, anticoagulant, antibacterial and antimicrobial agents has been intensively discussed [2,3]. Several studies also reported various methods to synthesizing Cu-NPs, including wet chemical reduction [4], thermal decomposition [5], microemulsion [6], solvothermal [7], sonochemical [8], and chemical reduction [7–11]. However, these methods have several disadvantages, such as the use of toxic chemicals, high costs, time-consuming process, and emission of hazardous by-products. The green synthesis method has become one of the most popular methods to produce nanoparticles in recent years and has several advantages, such as cost efficiency, biocompatibility, ease of use, usage of less toxic materials, and eco-friendly processes [9–11]. In recent years, there has been growing interest in the use of the green synthesis method, which utilizes natural resources,

such as plant extracts, fungi, bacteria, and algae to synthesize nanoparticles without producing any harmful by-products [12].

Several reports have been published based on the application of this method using extracts from plants, such as orange, lemon, and tangerine peel [13], *Ixoro coccinea* leaf [14], *Calotropis gigantea* [15], *Caccinia macranthera* [3,16], and *Lantana camara* [17]. These extracts were used as reducing agents to synthesis of nanoparticles due to the presence of metabolic compounds involved in bio-reduction process [18]. Reference [19] successfully synthesized CuO nanoparticles with a particle size of 20–35 nm using herbal tea (*Stachys Lavandulifolia*) flowers as a bio-reductor. The results showed that the tea contains polyphenolic compounds, which were believed to act as a reducing agent and have a high effect on C-heteroatoms coupling reaction catalyst.

Indonesia has actively enhanced the production of dragon fruit (*Hylocereus costaricensis*) with more than 370 tons/ha/year, which was consumed by the community and causes many peels to be wasted. Previous studies showed that the peel of red dragon fruit contains abundant reducing agents such as high levels of polyphenols, flavonoids, tannins, alkaloids, steroids, and saponins [20–22]. The utilization of red dragon fruit pulp extract has been successfully used previously as a bio-reductor for gold nanoparticle synthesis [23]. Therefore, its peel can be considered as a potential bio-reductor precursor for green synthesis of Cu-NPs.

Stabilizers play an important role to prevent the aggregation of nanoparticles. Polyvinyl alcohol (PVA) is a transparent polymer that can act as a stabilizer due to its ability to prevent agglomeration and undesirable oxidation processes [24]. El-Sayed [25] reported that the structure, optical, and electrical properties of Cu nanoparticles can be controlled by adjusting the PVA concentration.

The application of Cu-NPs as photocatalysts for photodegradation has gained a lot of attention, specifically as an isolated noble metal photocatalyst, namely Cu in the form of CuO. This form can act as light absorbers, catalytically active sites, and direct plasmonic photocatalysts [26]. However, CuO can be used as photocatalysts, which are associated with some limitations, such as low band gap and photo corrosion [27]. The application of nanoparticles as photocatalyst has been studied previously. Previous study reported the use of CeO nanoparticles in the photodegradation of methyl orange, rhodamine B, and methylene blue dyes in the presence of UVA light source [12]. The results demonstrated the satisfying photocatalytic activity for dyes water pollutants.

Nanoparticles possess exceptional quantum and surface properties, which enable them to improve their electrical, magnetic, and optical properties, and serve as effective photocatalyst [28]. Furthermore, one of the key factors that contribute to their catalytic ability is the increment in band gap (E_g). The value of E_g is very important for excitation of electrons from valence band (VB) to the conduction band (CB), thereby leaving holes (h^+). The $e^- - h^+$ pairs formed generated hydroxyl (OH•) and superoxide anions (O_2^-•) radicals, which react with dye molecules and ultimately degrade them [29].

Based on findings, there are no studies on the application of Cu-NPs in the photodegradation process, which were synthesized using red dragon peel extract. Therefore, this study aims to determine the effect of bio-reductors and precursor ($CuSO_4$) ratio on the characteristics of Cu-NPs and their efficiency as a photocatalyst in the AO7 dyes degradation process.

2. Materials and methods

2.1. Materials

The materials used in this study were 2 kg of red dragon fruit peel waste, 0.1 M $CuSO_4$ (Emsure Merck), PVA, ethanol (Emsure Merck), deionized (DI) water (Waterone), and AO7 dyes ($C_{16}H_{11}N_2NaO_4S$, CAS Number: 5850-86-2).

2.2. Preparation of plant extract

Red dragon fruit peel was used as the source of bio-reducing agent, which were extracted using a method developed in a previous study [23]. Fresh samples were purchased from a local market, thoroughly washed with DI water to remove surface impurities, and then finely crushed. Subsequently, 40 g of fine dragon fruit peel was added to DI water for extraction and boiled at 65 °C for 15 min, and the extract was separated with the filtration method.

2.3. Synthesis and characterization of Cu-NPs

Extract of dragon fruit peel and CuSO4 solution were mixed at a ratio of 1:1, 1:2, 1:3, and 1:4 (v/v). A total of 60 mL PVA 1% (v/v) was added to the mixture and stirred for 2 h, followed by resting for 1 h until a precipitate was formed. Subsequently, the precipitate was separated and dried at 100 °C and 250 °C for 45 min to obtain a shiny black powder. The samples were labeled as Cu-NPs (x), where x referred to the ratio of the mixtures. To examine the effect of PVA, Cu-NPs (1:1) without PVA were

also prepared. The synthesis procedure of Cu-NPs using dragon fruit peel extract is illustrated in Fig. 1.

FTIR (IR Prestige-21 Shimadzu) with the transmittance method (used KBr pellet) was employed to identify the possible bioactive molecules in the red dragon fruit peel extract and Cu-NPs. Furthermore, the spectrum was recorded at wavelength intervals of 4000 to 500 cm^{-1}. The crystallinity of Cu-NPs was evaluated using a powder X-Ray diffractometer (XRD, Shimadzu 7000) with CuKα radiation $\lambda = 1.5405$ Å) operated at a scanning range of 20—80 configuration. The crystallite domain size was calculated using the Debye—Scherrer equation. Surface textural properties were then determined through nitrogen adsorption using a surface area analyzer (SAA, type Quantachrome Nova 4200e) at a temperature of 273 K and the pretreatment was carried out at temperature of 250 °C with outgas time of 3 h. Brunauer-Emmet-Teller (BET) was used to calculate the surface area and pore volume. The t-Plot approach was used to calculate the total adsorbed gas at relative pressure $P/P_o = 0.99$ which represent the total pore volume. The surface morphology of Cu-NPs powder was captured using the scanning electron microscope (JEOL JSM 6063LA) operated at an accelerated voltage of 130 kV.

2.4. Photocatalytic properties of Cu-NPs

Photocatalytic properties of Cu-NPs were evaluated with the degradation of AO7 dyes in an aqueous solution. The process was carried out by adding 0.05 g of Cu-NPs into 50 mg L^{-1} AO7 solution with a pH of 9 [30]. It was then irradiated with a UV lamp (Philips TUV 15W/G15 T8 - λ 280 nm) on the photocatalytic reactor system, as shown in Fig. 2. Furthermore, 5 mL of solution was removed every 30 min to measure the absorbance using a Shimadzu UV-Vis spectrophotometer. The percentage of photodegradation (%D) was calculated based on Equation (1) [16,31].

$$\%D = \frac{C_0 - C}{C_0} x 100\% \tag{1}$$

Where %D is the percentage of photodegradation, C_0 is the initial concentration, and C is the concentration after photodegradation at time t.

The reuse test of Cu-NPs was conducted by recycling the materials and utilized them for several cycle. The recycling procedure was performed by washing Cu-NPs in methanol with stirring for 1 h and dried at 100 °C for 12 h.
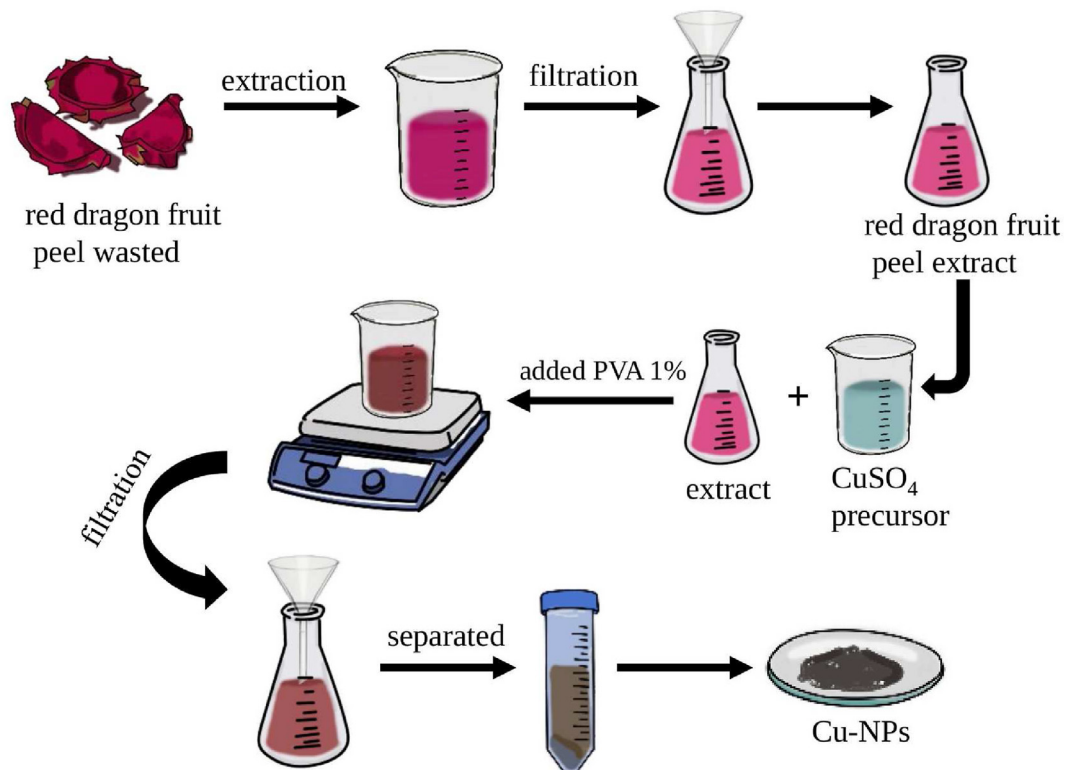

Fig. 1. The illustration of biosynthesis Cu-NPs using red dragon fruit peel extract.
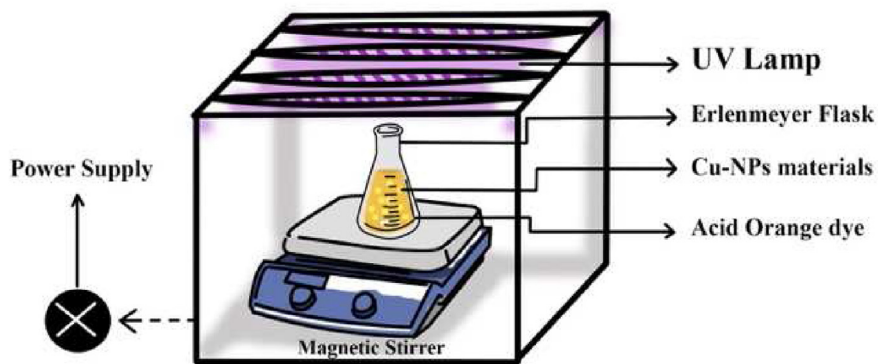
Fig. 2. The schematic diagram of the photocatalytic reactor system.

Subsequently, the Cu-NPs that were used for the degradation of AO7 dyes was tested at the same experimental conditions.

3. Results and discussions

A fresh red dragon fruit peel were used as a bio-reductor for Cu-NPs synthesis without drying process because it can damage certain chemical compounds, which act as reducing agents.

Subsequently, the extract was mixed with Cu-precursor ($CuSO_4$) as a source of Cu^{2+}. The changing color of solutions are shown in Fig. 3. After the extract of red dragon fruit peel (Fig. 3a) was mixed with $CuSO_4$, the color changed from light red to dark red as shown in Fig. 3b. Furthermore, the solution then changed to green after 2 h of reaction. These changes occurred due to the reduction of Cu^{2+} ions to Cu^0 by the OH functional group in red dragon fruit peel extract, as indicated by the FTIR
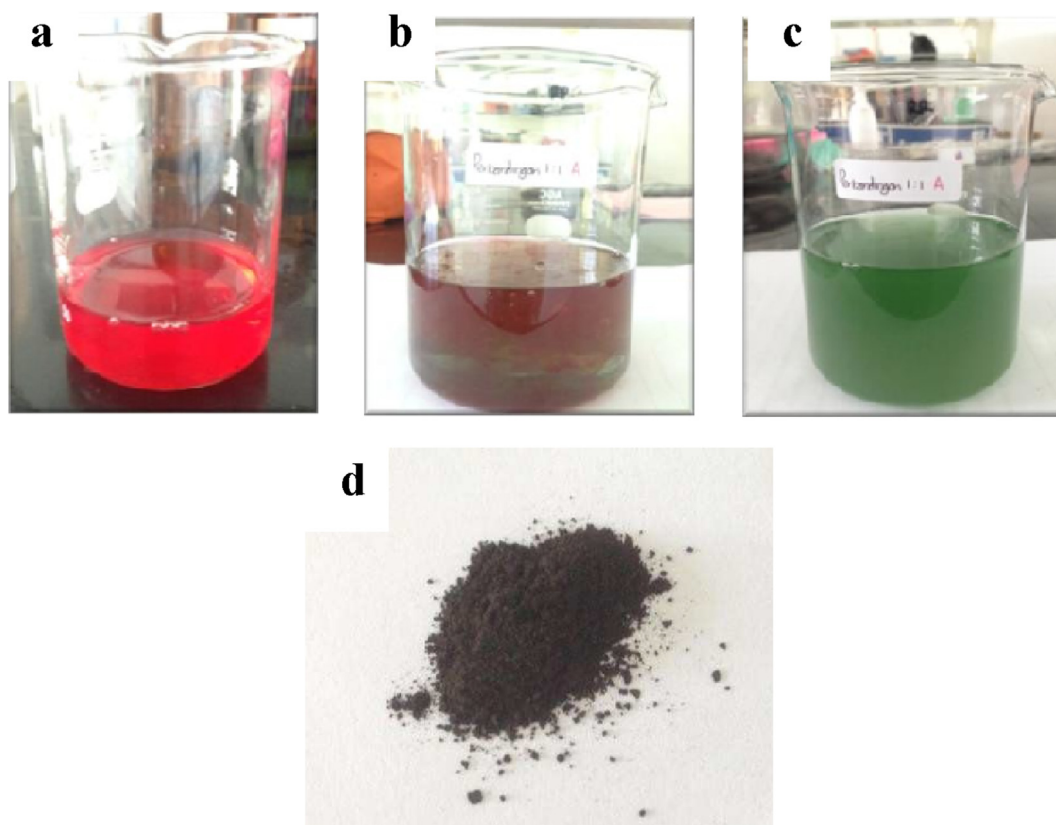

Fig. 3. (a) Bio-reductor of red dragon fruit peel extract, (b) solution of $CuSO_4$ and bio-reductor (1:1), (c) solution of $CuSO_4$ and bio-reductor after 2 h, (d) Cu-NPs powder (d).

analysis. A shiny black color of Cu-NPs was obtained after centrifugation and drying, as shown in Fig. 3d.

3.1. FTIR analysis

FTIR spectroscopy was employed to study the interactions between different species and changes in the chemical compositions of the mixture during biosynthesis [32]. Furthermore, FTIR analysis of the red dragon fruit peel extract and Cu-NPs was carried out to identify the possible biomolecules that are responsible for the reduction, capping, and efficient stabilization of the bio-reduced Cu-NPs. Fig. 4a shows IR spectra of red dragon fruit peel extract, where a broad and strong band at 3451.92 cm^{-1} represents −OH stretching vibration. The C−H stretching vibration of the methyl ester in galacturonic acid was attributed to the absorption bands in the vicinity of 2950 cm^{-1} [33]. The sharp peak at 1638.38 cm^{-1} corresponded to C=C groups, while the weak variant at 1165.22 cm^{-1} corresponded to C−O alcohol. The peaks showed the presence of the phenolic or alcoholic groups, and it supported that red dragon fruit peel extract contains several polyphenolics, flavonoids, and alkaloids (reductor), which play an important role in the bio-reduction process.

The spectrum of Cu-NPs with and without PVA (Fig. 4b and c) showed prominent wavenumbers at ~3424.35 cm^{-1}, ~2954-2850 cm^{-1}, ~1730 cm^{-1}, ~1630 cm^{-1}, ~1430 cm^{-1}, ~1110 cm^{-1}, and ~763 cm^{-1}, which are assigned as −OH, −CH$_3$, −C=O, −C=C, C−H vinyl, and C−O groups, respectively [34]. Furthermore, a strong band in the

region of 1000−1300 cm^{-1} indicated a C−O stretching in the phenolic or alcoholic group [35]. The spectrum of Cu-NPs with and without PVA generally showed a similar spectrum, indicating that the presence of PVA does not have a significant effect on the functional group of copper nanoparticles. The sharp peak at ~1110 cm^{-1} in Fig. 4b indicated the strong interaction of -C-O due to the presence of PVA. The peaks at ~614 cm^{-1} and ~476 cm^{-1} corresponded to Cu_2O and CuO, respectively [13,14]. These results indicated that phenolic/alcoholic group in red dragon peel extract can reduce $CuSO_4$ to form Cu^0 on nanometer scale.

The possible mechanism proposed for the reduction of Cu^{2+} to Cu-NPs involved the ability of copper ions to form intermediate complexes with phenolic −OH groups in flavonoid, which subsequently oxidized to form quinone and Cu^{2+} is reduced to Cu^0. The mechanism of the ion reduction reaction with flavonoid is presented in Fig. 5.

3.2. UV-Vis analysis

UV-Vis absorption spectroscopy has become a very useful technique to study the stability of metal nanoparticles owing to the peak positions and shapes are sensitive to particle size. Furthermore, PVA was used to maintain the stability of the nanoparticles in this study. The effect of PVA on Cu-NPs is shown in Fig. 6. The UV-Vis results revealed that with absence of PVA, the maximum wavelength changed significantly with increasing time. This indicated that the size of Cu-NPs was agglomerated to form a larger particle size, leading to the decrease of peak at 570 nm. The peak of Cu-NPs with addition of PVA shifted to 500 nm region and broadened at short wavelengths, indicating the presence of smaller separated Cu-NPs. This is in line with the results from previous studies utilizing ascorbic acid as a stabilizer [36]. However, Cu-NPs without PVA showed a peak around 570 nm. Based on the results, the presence of PVA increased the effective capping capacity, and this leads to the production of smaller copper nanoparticles [37]. This phenomenon will be discussed in more detail in the section on morphological analysis using SEM.

3.3. XRD analysis

The XRD spectra (Fig. 7) shows three distinct diffraction peaks at 43.3°, 50.4°, and 74.1° with index Miller of (111), (200), and (220), respectively, and this confirmed the face-centered cubic (FCC) Cu-NPs. Subsequently, the obtained data were matched
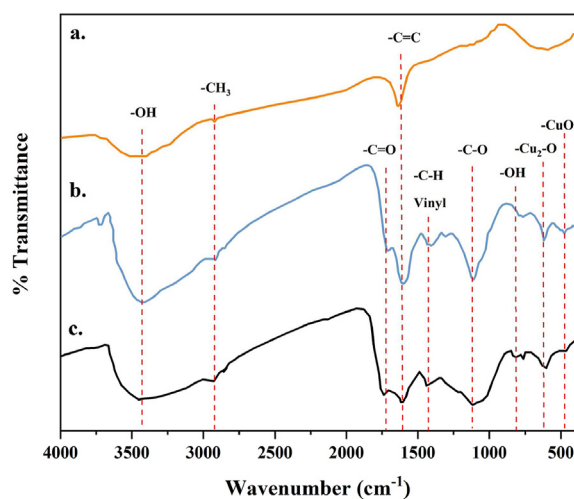

Fig. 4. FTIR spectra of (a) red dragon fruit peel extract, (b) Cu-NPs (1:1) with PVA addition, (c) Cu-NPs (1:1) without PVA addition.
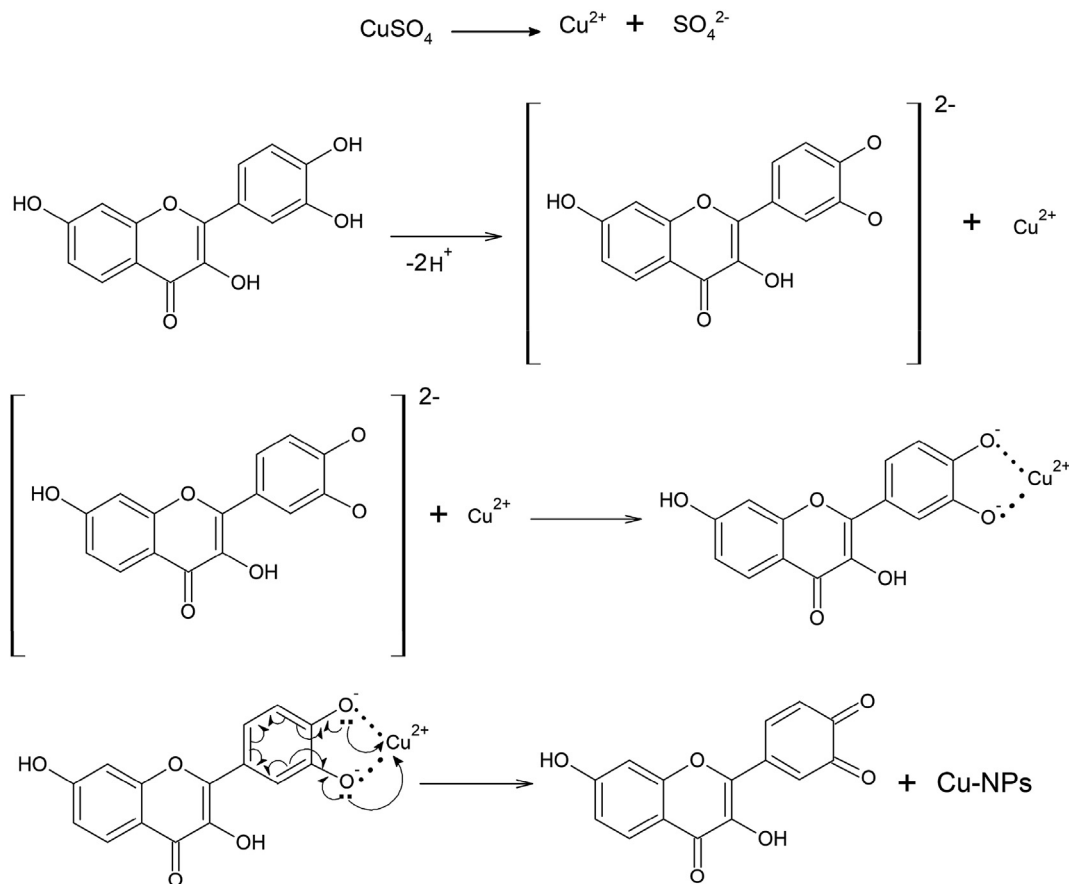
Fig. 5. The possible mechanism of formation Cu-NPs by −OH functional group from red dragon fruit peel extract.

with the Joint Committee on Powder Diffraction Standards (JCPDS) file number: 04—0836. Similar observations have also been reported by previous studies [9,32,38]. The presence of peaks around $2\theta = 37°, 39°, 62°, 64°$ indicates the oxidation from Cu^0 to CuO or Cu_2O with a monoclinic structure [24,39].

The average crystallite size of Cu-NPs was calculated using Debye Scherrer's, as shown in Equation (2) [40].

Fig. 6. The UV-Vis absorption spectra of Cu-NPs (1:1) with PVA addition (a) and without PVA addition (b).

Fig. 7. The XRD pattern of Cu-NPs.

$$D = \frac{0.98\lambda}{\beta \cos \theta} \qquad (2)$$

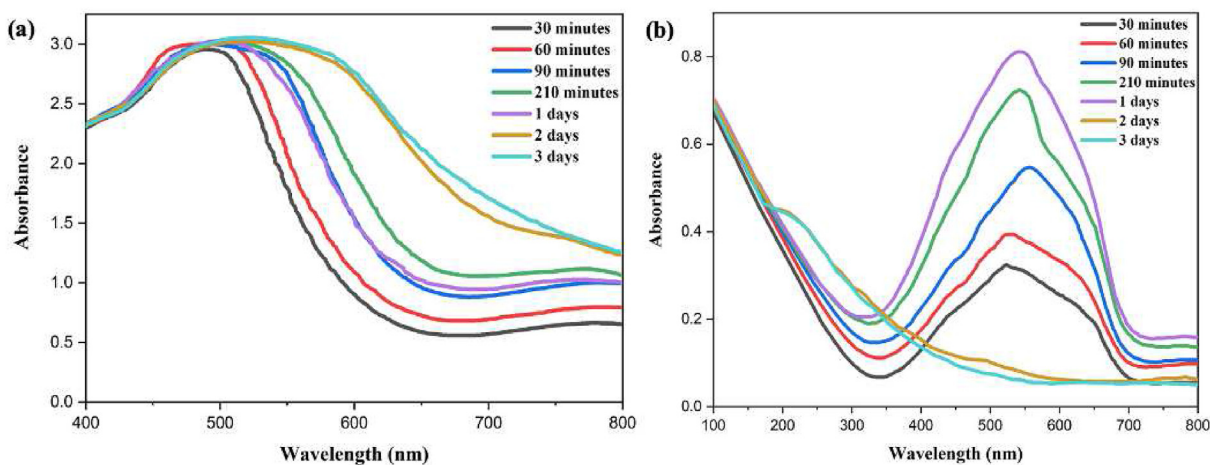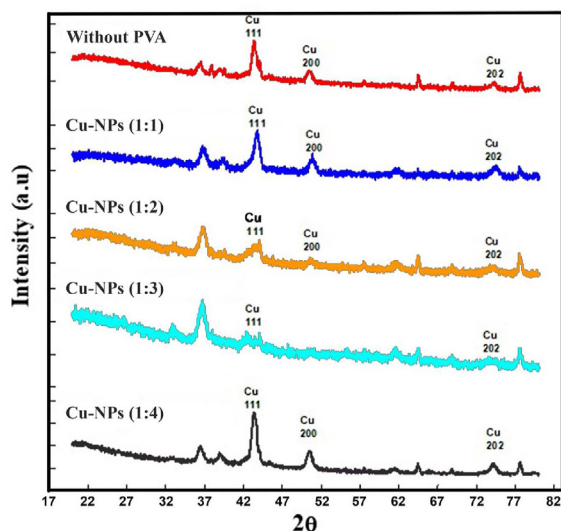Where 0.98 was a constant value known as a shape factor, λ is the wavelength of the X-rays and taken as 1.54, β is FWHM (full Width at half maximum) of the diffraction peaks and θ is the diffraction angle. Based on the results in Table 1, Cu-NPs with a ratio of 1:2 had the smallest average crystallite size of 8.65 nm. Furthermore, the particle size of Cu-NPs (1:1) with PVA (9.74 nm) was smaller than without PVA (12.44 nm). This result indicated that the bio-reductor ratio had no influence on the crystallite size of Cu-NPs, but the presence of PVA can hinder the agglomeration of Cu^0 particles, leading to smaller sizes.

3.4. SEM analysis

The SEM images of Cu-NPS revealed that all samples had a spherical shape, as shown in Fig. 8. Cu-NPs tended to aggregate due to their high surface free energy, but individual nanoparticles can also be detected, as shown in Fig. 8. Furthermore, the SEM images of Cu-NPs synthesized using PVA revealed that each of the materials has a consistent shape, indicating a crystalline structure. The homogenous nucleation process caused by the reduction of Cu^{2+} to Cu^0 was responsible for the production of Cu-NPs structure. It is also led the formation of the initial mono-crystalline nano-sized clusters of Cu-NPs [41].

The particle size of Cu-NPs and its structure can be controlled by the presence of PVA, yet the particle size without PVA became larger, causing a tendency to be clustered, as shown in Fig. 8e. The occurrence of agglomeration in nanoparticles indicated the role of PVA as a stabilizing agent for nanoparticle size. This finding was supported by the UV-Vis analysis spectra (Fig. 6), which showed a decrease in absorbance with increasing storage time.

The diameter distribution of Cu-NPs is presented in Fig. 9, which the size ranged from 10 nm to 80 nm. Furthermore, the size larger along the amount of precursor $CuSO_4$ and Cu-NPs without PVA became larger. The diameter obtained in this study was larger compared to Cu-NPs synthesized using *Celastrus paniculatus* extract [42]. The average size of the products showed a trend toward growth due to the addition of PVA. This critical discovery showed the crucial role of the additive in regulating particle size. The Cu-NPs' diameter distribution in this

Table 1. The XRD analysis of Cu-NPs.

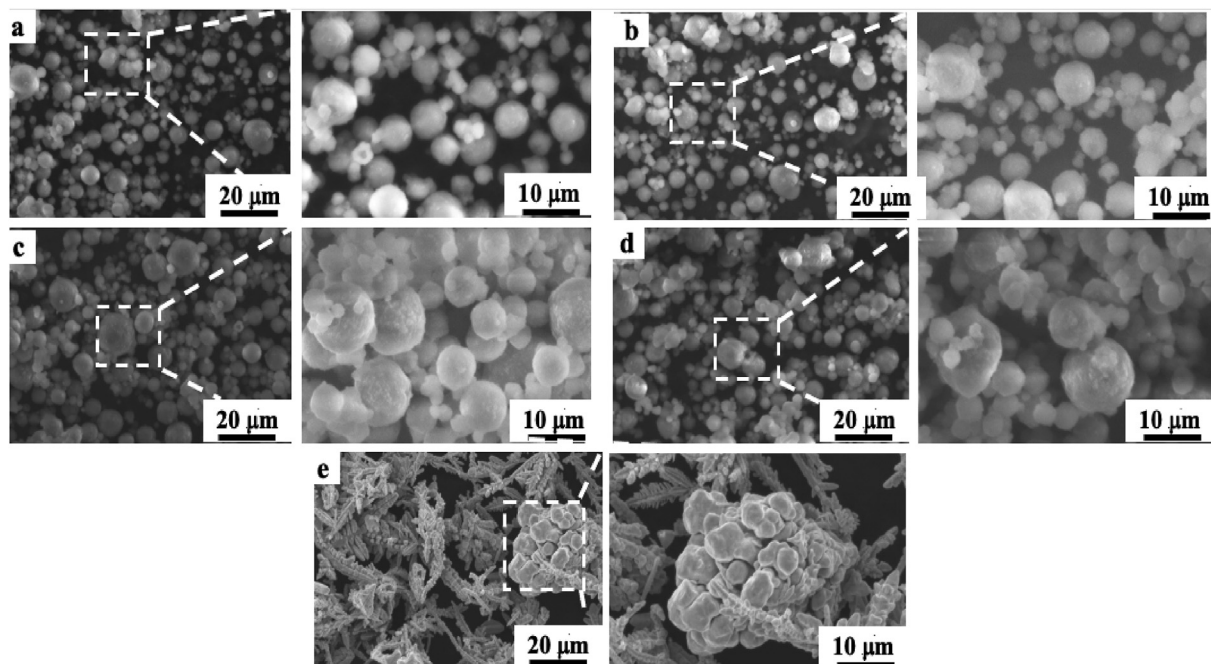| Samples	hkl	2-Theta (°)	Crystallite size (D) (nm)	Average of crystallite size (nm)
Cu-NPs (1:1)	111	43.65	9.94	9.74
	200	50.75	9.43	
	220	74.33	9.86	
Cu-NPs (1:2)	111	43.36	5.16	8.65
	200	50.59	11.49	
	220	73.94	9.31	
Cu-NPs (1:3)	111	43.80	8.86	8.85
	220	73.81	8.84	
Cu-NPs (1:4)	111	43.34	11.31	11.22
	200	50.43	10.03	
	220	74.06	12.32	
Cu-NPs (1:1) without PVA	111	43.31	13.35	12.44
	200	50.43	10.52	
	202	74.07	13.45	

Fig. 8. SEM image of Cu-NPs with ratio of bio-reductor and precursor CuSO₄ (a) 1:1, (b) 1:2, (c) 1:3, (d) 1:4, (e) 1:1 without PVA.

study was larger compared to those produced using surfactants Tween-80 [41].

The EDS analysis confirmed the quantitative composition and stability of the Cu-NPs, as shown in Fig. 10a. The purity levels of the particles were evaluated, and the results showed that red dragon fruit peel extract-mediated Cu-NPs had 99.05% mass of Cu, and some weak signals of C, N, Ca, and O. Furthermore, these weak signals were responsible for the presence of macromolecules in the extracts, such as flavonoids, phenolic, polysaccharides, glycosides, steroids, and tannins, and emitting X-rays [42]. The homogenous distribution of Cu on the surface of the sample is depicted in Fig. 10b.

3.5. Surface area analysis

To investigate the surface area of Cu-NPs N_2 adsorption−desorption was tailored. The results showed that the shape of the adsorption−desorption was the same for all samples, as shown in Fig. 11 and Table 2. According to the Brunnauer-Deming-Teller classification, the adsorption isotherm for all samples was close to Type IV. Furthermore, this was characterized by a hysteresis loop at higher partial pressures and a little amount of adsorption occurring at low levels. This type of isotherm was assigned in several mesoporous solids materials. Monolayer-multilayer adsorption was responsible for the Type IV isotherm's first portion, while capillary condensation occurred in mesopores causes the isotherm's hysteresis loop [43,44].

Based on Table 2, the ratio of bio-reductors and $CuSO_4$ had no effect on the pore volume, which was around 0.20 cc g^{-1}. However, it had a significant effect on the surface area, which increased from 250 m^{2}g^{-1} (1:1) to 278.85 m^{2}g^{-1} (1:3) and then decreased to 244.38 m^{2}g^{-1} (1:4). Furthermore, the volume of micropore is ranged from 0.12 to 0.14 cc g^{-1} while mesopore volume is constant (0.08 cc g^{-1}). This phenomenon can be attributed to the sample average crystal size from the results of XRD analysis, where the larger the crystal size, the lower surface of Cu-NPs [45]. This trend was supported by the diameter distribution (Fig. 9), where higher surface area was associated with smaller diameter distribution of Cu-NPs. Furthermore, this has important implication for photocatalytic activity as a higher surface area can improve the efficiency of photogenerated charge separation and overall performance [46]. The surface area produced in this study was larger compared to that of Cu-NPs produced using the chemical reduction method [47]. Based on these characteristics, the Cu-NPs obtained can be used as photocatalytic for dye degradation.
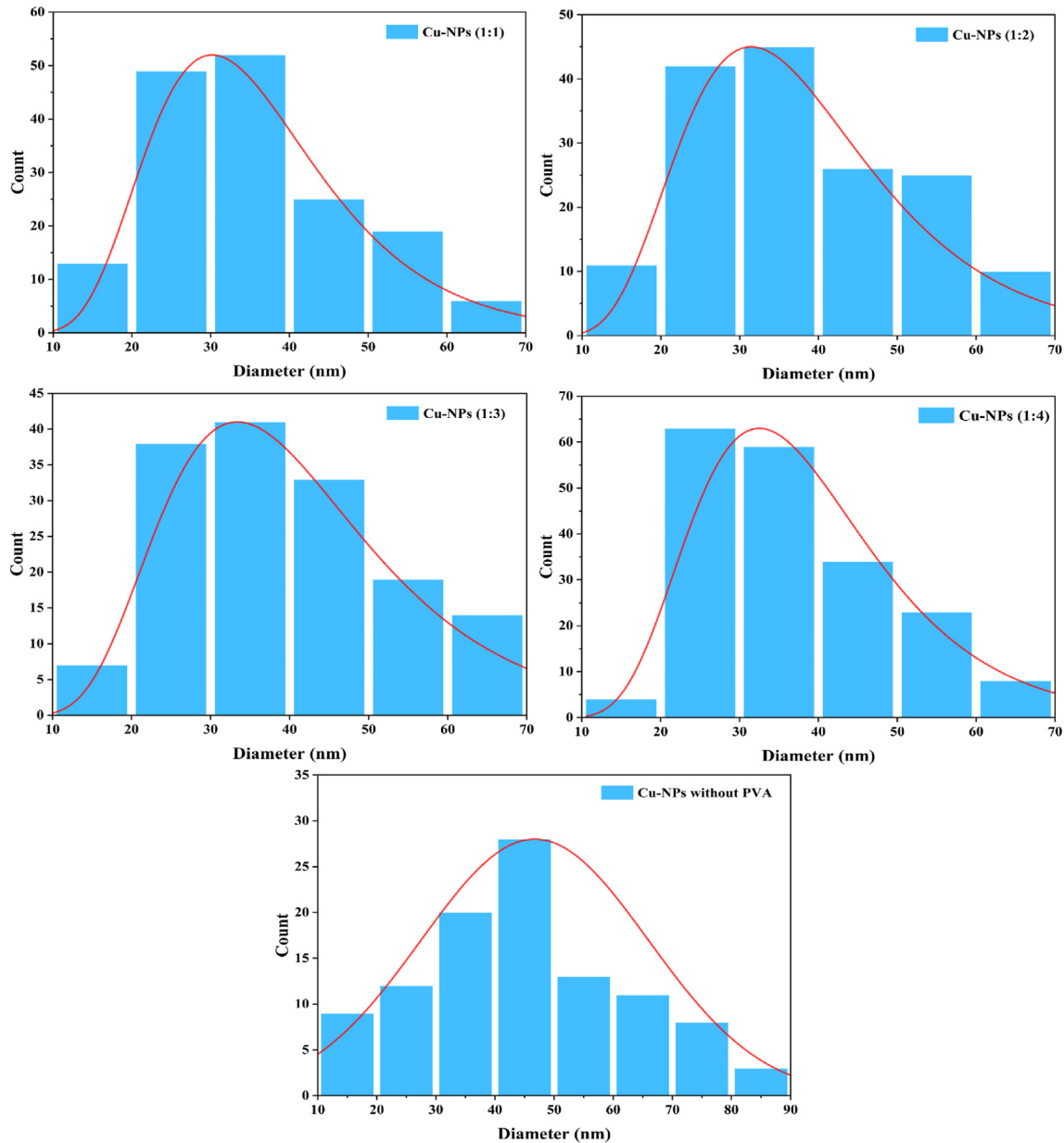
Fig. 9. Plot of the diameter distribution of Cu-NPs.

3.6. Photocatalytic properties

The photocatalytic degradation of AO7 was examined to explain the properties of Cu-NPs. The absorption spectra were employed to investigate the energy band and the kind of electronic transitions, as shown in Fig. 12a. Furthermore, the spectra of Cu-NPs showed a prominent absorption edge of approximately 410 nm, which was caused by an indirect transition of electrons [48].

The bandgap (Eg) in this study was calculated using Tauc's plot, which is the relationship between the absorption coefficient (α) and incident photon energy (αhv), as shown in Equation (3) [12].

$$\alpha hv = A(hv - Eg)^n \tag{3}$$

where h is Planck's constant (6626 x 10^{-34} J s), v is the frequency of light, c is the velocity (3 x 10^8 ms^{-1}), and n is 2 for indirect semiconductors. Fig. 12b shows the Eg of Cu-NPs for all samples by extrapolating the linear portion to the photon energy axis. The calculated direct Eg value for all samples in this study was 2.49−2.74 eV. This value was similar to
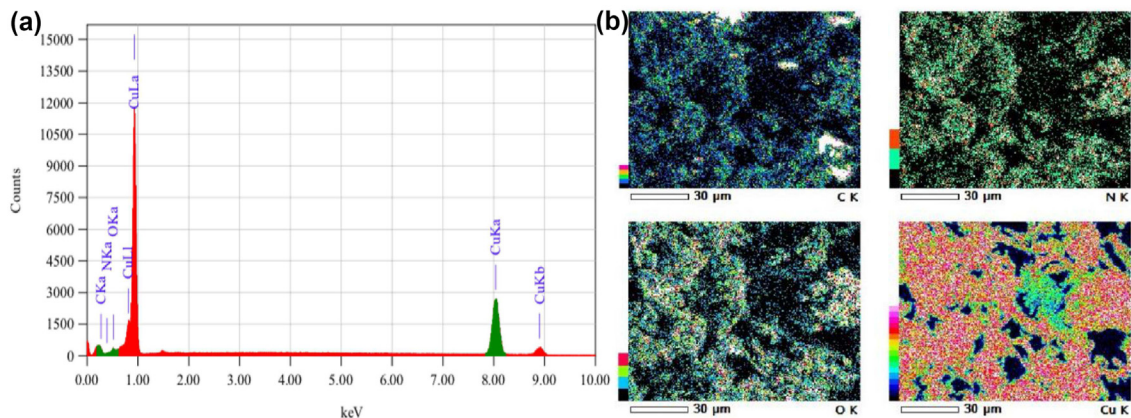
Fig. 10. The EDS (a) and Mapping elemental (b) of Cu-NPs (1:1).

that of Cu-NPs synthesized using *Moringa Oleifera* leaf extract [49], but was lower compared to those produced with the electrodeposition method [50]. This findings is consistent with a previous study, which reported an increase in the Eg of bio-synthesized nanoparticles compared to those chemically synthesized [3]. The increase in Eg was caused by the existence of intragap states and the quantum confinement effect.

Fig. 12c depicts the variation of the absorption coefficient in Cu-NPs as a function of photon energy. Furthermore, the graphic unequivocally demonstrates that as wavelength increase, the absorption coefficient tended to decrease exponentially. This

behavior is common in several semiconductors and can be induced by various factors, including internal electric fields within the inelastic scattering of charge carriers by phonons and the lattice deformation caused by strain from imperfections [48,51].

Based on the Eg value, Cu-NPs have the potential to be used as a photocatalyst in the AO7 dye degradation process. The photocatalytic degradation efficiency was determined with a spectrophotometer at 580 nm, as shown in Fig. 13. At a basic pH of 9 and the presence of Cu-NPs, photodegradation was dramatically accelerated. The anionic dye molecule of AO7 was negatively charged and it is adsorbed on the photocatalyst surface, and this
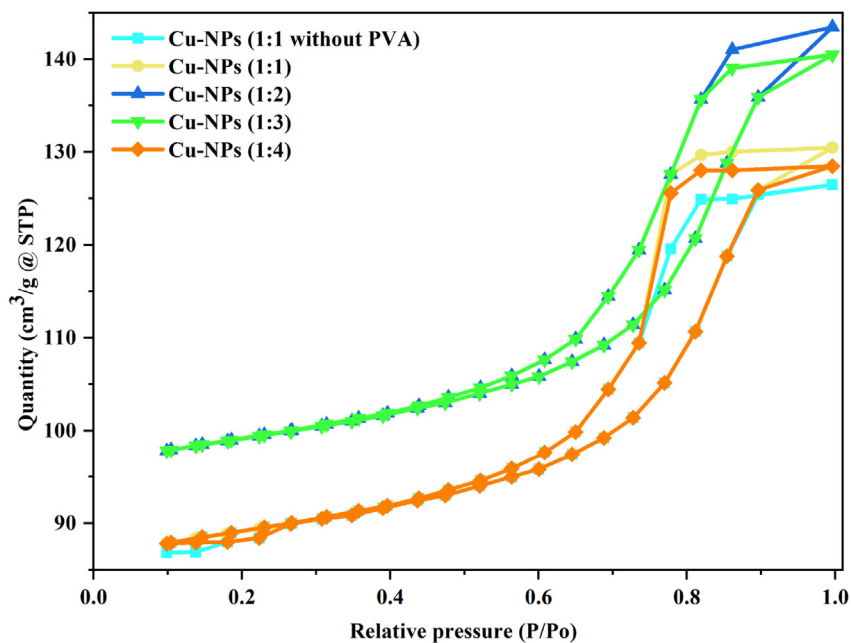

Fig. 11. N_2 adsorption and desorption isotherms of Cu-NPs.

Table 2. Surface area analysis of Cu-NPs (correspond from Fig. 9).

Samples	Surface Area (m²g⁻¹)			Volume @STP (cc g⁻¹)		
	[a]BET	[b]Micro	[c]Meso	[d]Total	[e]Micro	[f]Meso
Cu-NPs (1:1)	250.00	220.48	29.52	0.20	0.12	0.08
Cu-NPs (1:2)	277.07	247.55	29.52	0.22	0.14	0.08
Cu-NPs (1:3)	278.85	249.33	29.52	0.22	0.14	0.08
Cu-NPs (1:4)	244.38	214.86	29.52	0.20	0.12	0.08
Cu-NPs (1:1) without PVA	227.75	198.23	29.52	0.19	0.12	0.07

[g]Pore distribution based on BJH analysis.
[a] BET surface area.
[b] Micropore surface area evaluated by t-plot method.
[c] Mesopore surface area calculated using S_{BET}-S_{micro}.
[d] Total pore volume at P/Po ~ 0.99.
[e] Micropore volume calculated by t-plot method.
[f] Mesopore volume calculated using V_{total}-V_{micro}.

altered the surface charge characteristics of the catalyst under basic conditions [42].

The degradation efficiency of different catalyst was calculated based on Equation (1) and plotted in Fig. 14, which demonstrated the effectiveness of Cu-NPs in degrading AO7 under UV and non-UV conditions. There was no degradation process of AO7 in the absence of Cu-NPs and in dark conditions without UV. However, under UV light the degradation percentage reached 18.16%. This low efficiency can be attributed to water photolysis reactions, in which H_2O molecules were decomposed
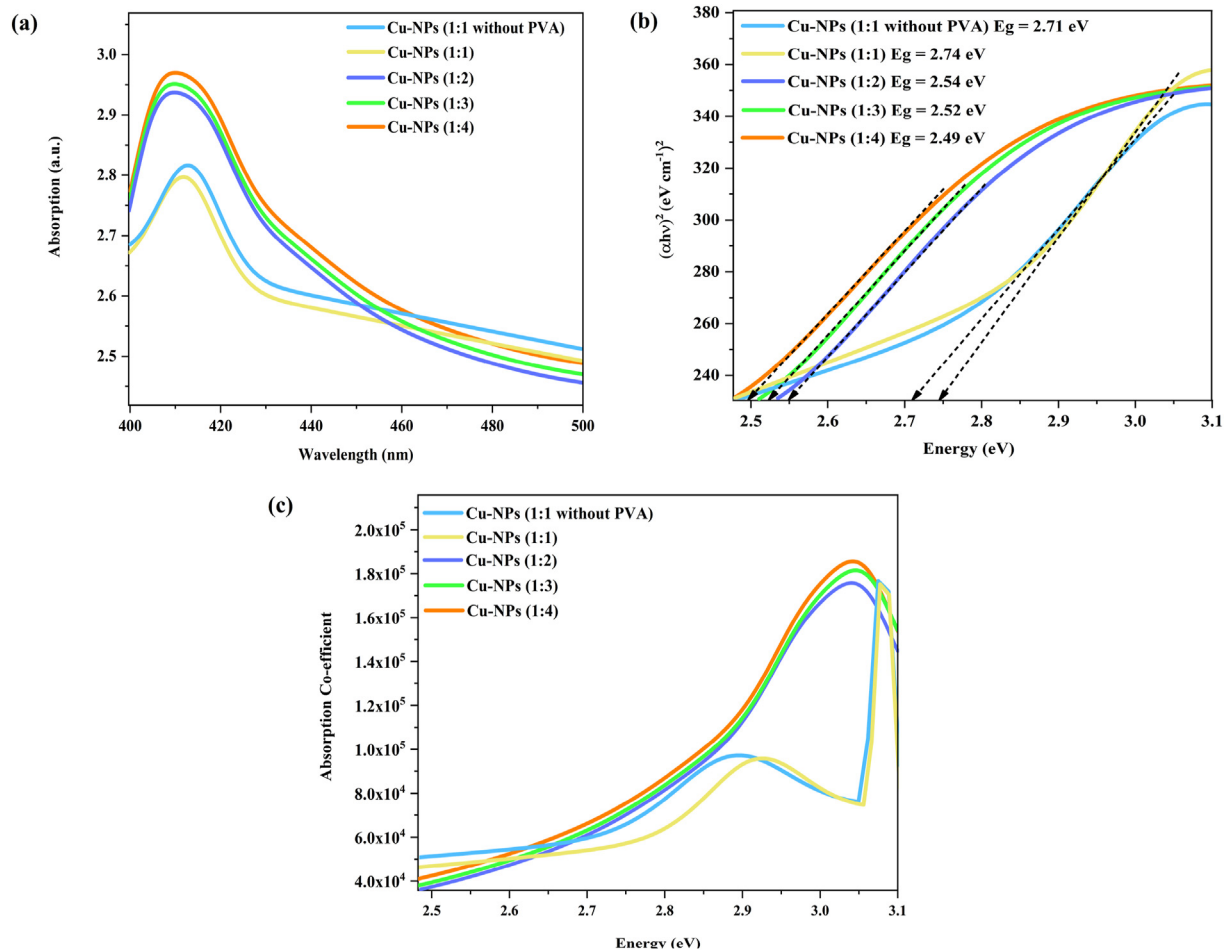

Fig. 12. Optical properties of Cu-NPs: UV absorption (a), band gap (b), absorption coefficient (c).
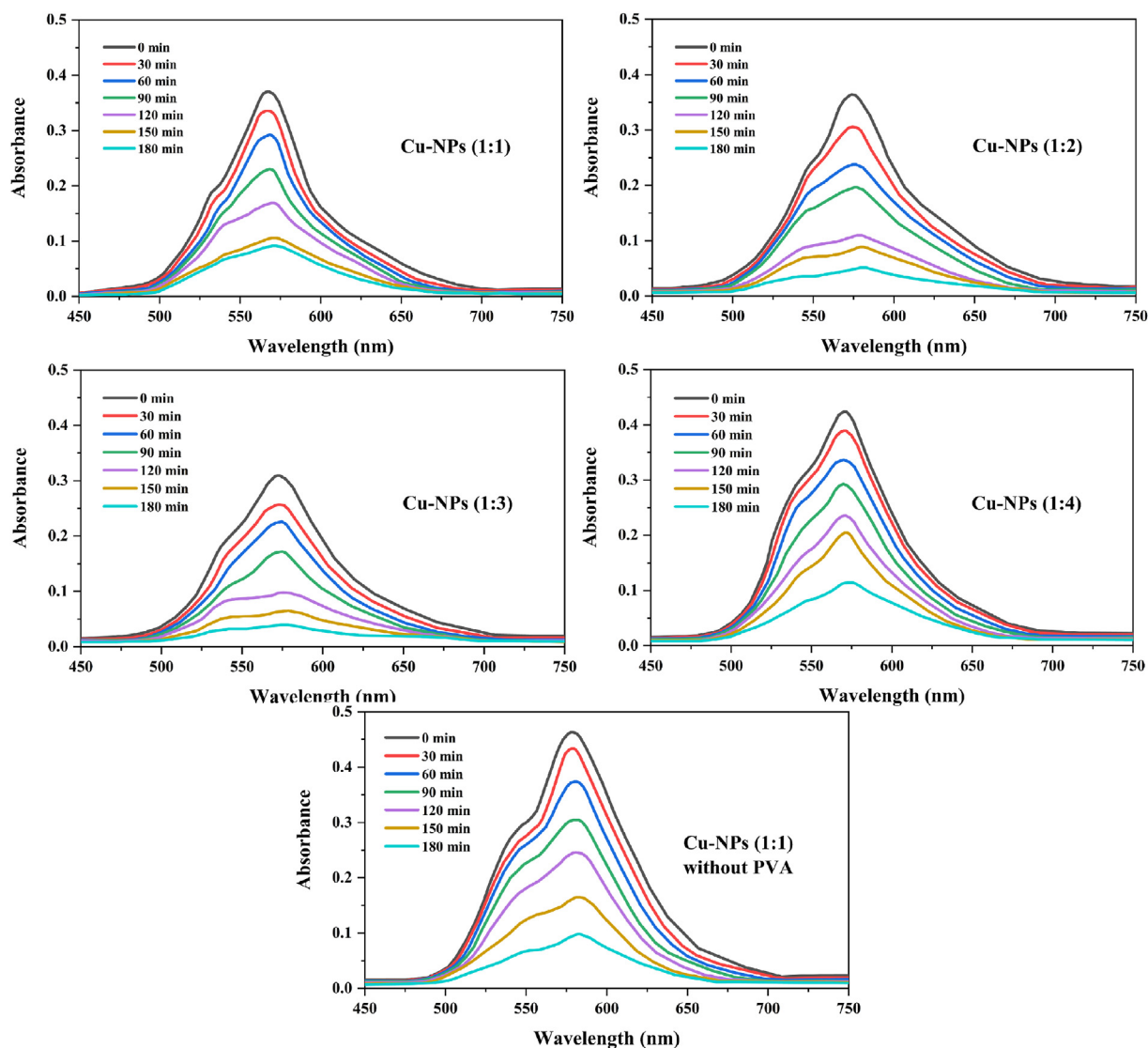
Fig. 13. The photocatalytic degradation of AO7 as a function of irradiation time using Cu-NPs.

after absorbing photons to produce •OH and H$^+$. The degradation efficiency almost similar to the use of Cu-NPs without UV, suggesting that process was driven by the absorption of AO7 onto the surface of the nanoparticles. This was supported by Table 2 showing that Cu-NPs produced have high surface are and pore volume.

The use of Cu-NPs (1:3) under UV light led to an excellent degradation efficiency of 81.07%. This can be attributed to several factors, including the low Eg, the high porosity, and the large surface area. These properties facilitated the formation of OH• radicals under UV light. Furthermore, the increased specific surface area and porosity of Cu-NPs provided numerous reactive sites and promoted electron separation from holes, thereby accelerating photocatalytic activity [46]. Another important factor is the alkaline conditions in which the photodegradation process occurred, leading to high concentration of OH$^-$ ions on the catalyst surface. The abundance of OH- ions may promote the abundance OH• radicals and accelerate the photodegradation process [52]. Furthermore, the small particle size, low Eg, and large surface area act optimally to ensure that the electrons were effectively excited to the surface of the catalyst leading to the enhancement the efficiency of degradation. The results confirmed from previous study which reported that the photocatalytic effect depended on the size and surface of particles [53].
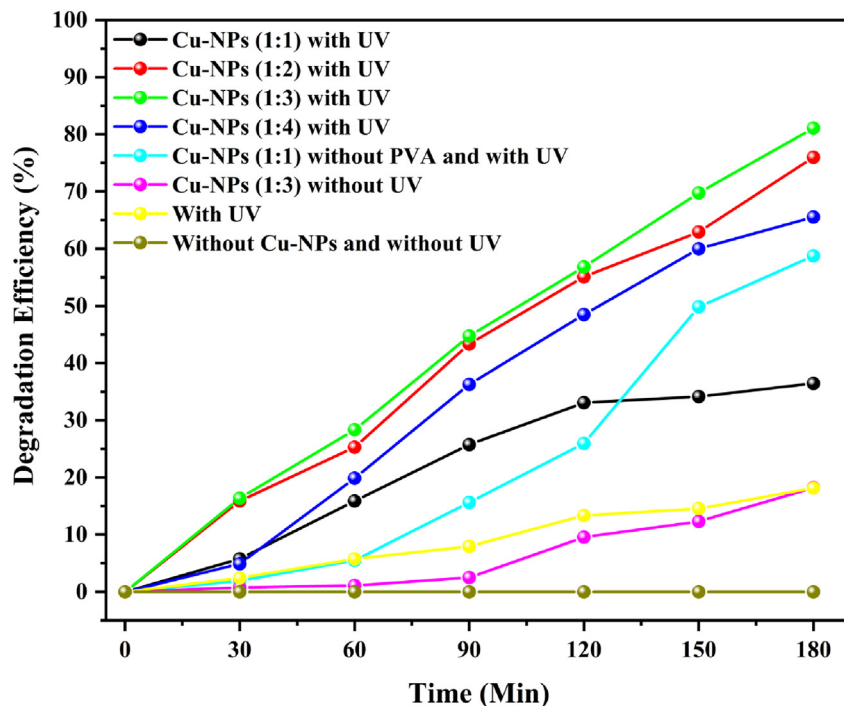
Fig. 14. The photocatalytic degradation efficiency of AO7 using Cu-NPs.

A pseudo-first-order reaction was used to characterize the kinetics of the photocatalyzed process for AO7 dye, based on Equation (4).

$$\ln\frac{C_t}{C_0} = -kt \qquad (4)$$

where C_0 is the initial concentration, C_t is the AO7 concentration at the irradiation time (t), and k is the rate constant (min^{-1}). Based on the values of the correlation coefficient ($R^2 > 95$), the linear relationship between $\ln(C_t/C_0)$ and irradiation time (t) was well correlated, as shown in Fig. 15. The slope of the linear fitting line showed that the reaction's rate constant (k) ranged from 0.0027 to 0.0089 min^{-1}. Based on these findings, the AO7 dye degraded over a period of 180 min, with pseudo-first-order kinetics. Furthermore, a rate constant of 0.0089 min^{-1} was obtained for Cu-NPs (1:3), which has a high degradation efficiency.

Reusability is an important parameter for photocatalytic applications, hence, Cu-NPs (1:3) was chosen to evaluated the reusability of Cu-NPs due to it performed the highest degradation efficiency and it displayed in Fig. 16a. The result shows that the photocatalytic activity decreases from 81.07% to 55.01% after four cycles. The results also revealed that there was no photo corrosion during the photooxidation of AO7. Furthermore, the minor

reduction observed was caused by the permanent attachment of dye or other intermediates molecule on the surface of Cu-NPs hindering the adsorption of photon and AO7 molecules, hence, this leads to loss its ability to perform photocatalytic in many cycle or reuse [54]. The low number of cycles of the degradation process in Cu-NPs samples is also caused by the powder form of the nanoparticles, which catalyst leaching is easily taken place [31]. However, the number of cycles produced was greater compared to previous study using TiO$_2$ nanoparticles [55].

The mineralization process of AO7 compounds was carried out to confirm the occurrence of degradation by measuring TOC removal for each cycle, as shown in Fig. 16b. Based on previous study [56] the Cu-NPs species, which are an electron scavenger, causes the semiconductor–metal Schottky barrier to form at the contact region, assisting in charge separation and improving photoactivity performances. The results explained the increase in TOC removal from each cycle up to 39.14% in the fourth cycle. This is consistent with the results of previous studies, where an increase in percent removal indicated the progress of mineralization. This process was caused by the conversion of aromatic compounds into aliphatic compounds through ring–opening reactions [57].
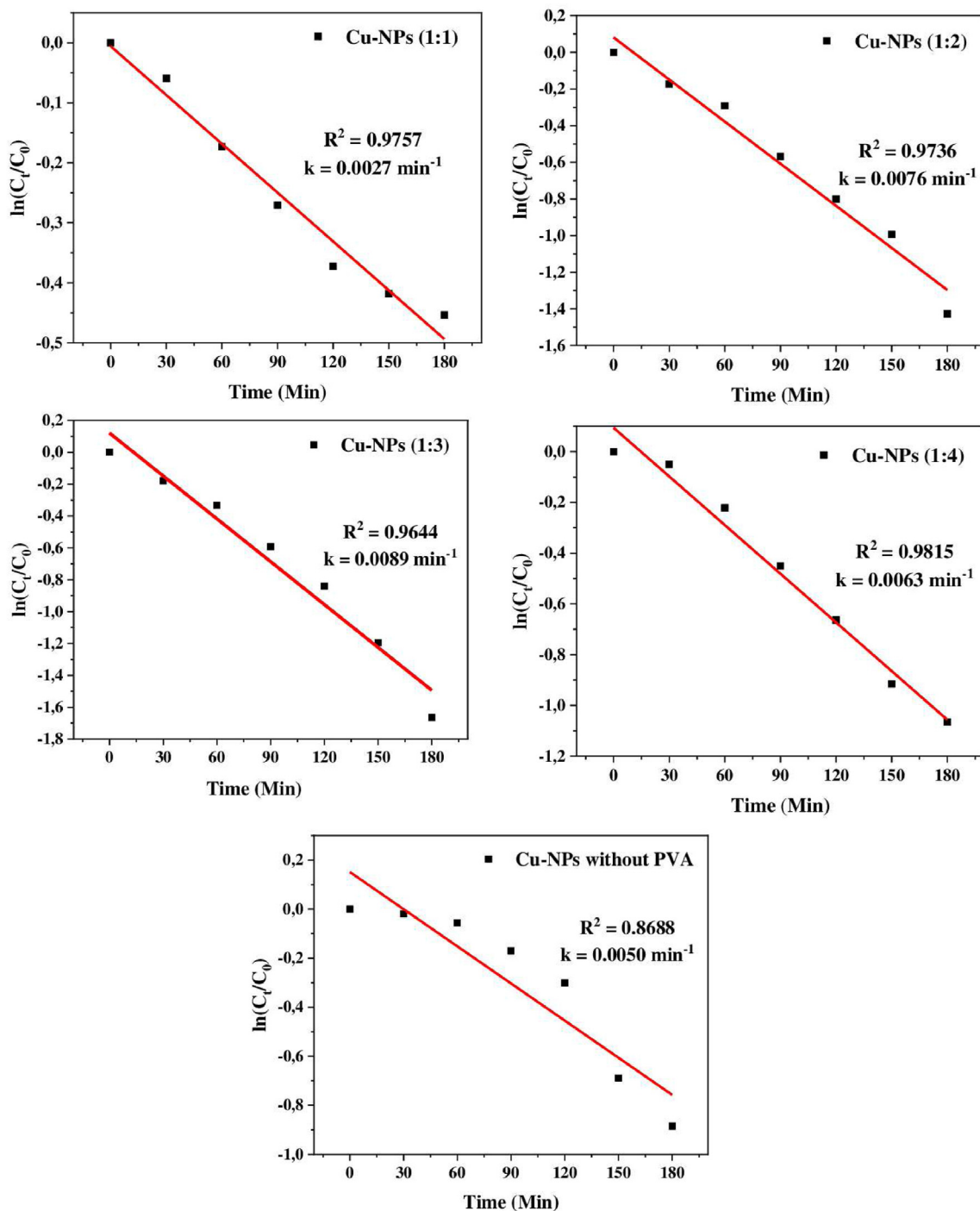
Fig. 15. Kinetic data for the degradation of aqueous AO7 using Cu-NPs.

Furthermore, the possible degradation mechanism provided in this study is presented in Fig. 17. In this mechanism, H_2O molecules reacted with the holes (h^+) in VB to produce $OH^•$ radicals, while O_2 interacted with the electrons in CB to produce O_2. The active radicals can sequentially chain-react to destroy the AO7 dye [16]. The ability of radicals to transform organic molecules into CO_2, H_2O, NO_3, and a variety of ions as by-products determined the effectiveness of this approach for breaking down AO7 dye [58]. A comparison of the photocatalytic reduction of AO7 utilizing various nanoparticles for the latest study is shown in Table 3.

Fig. 16. The reusability of Cu-NPs (1:3): as a degradation efficiency (a) and the TOC removal (b).

Fig. 17. The possible mechanism of AO7 degradation using Cu-NPs synthesized using red fruit dragon peel extract.
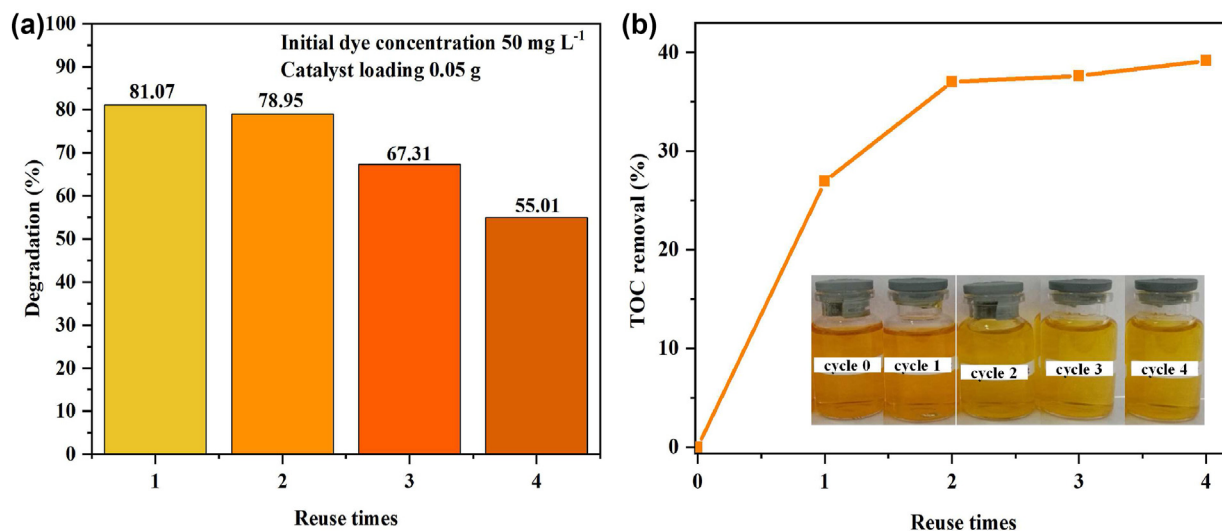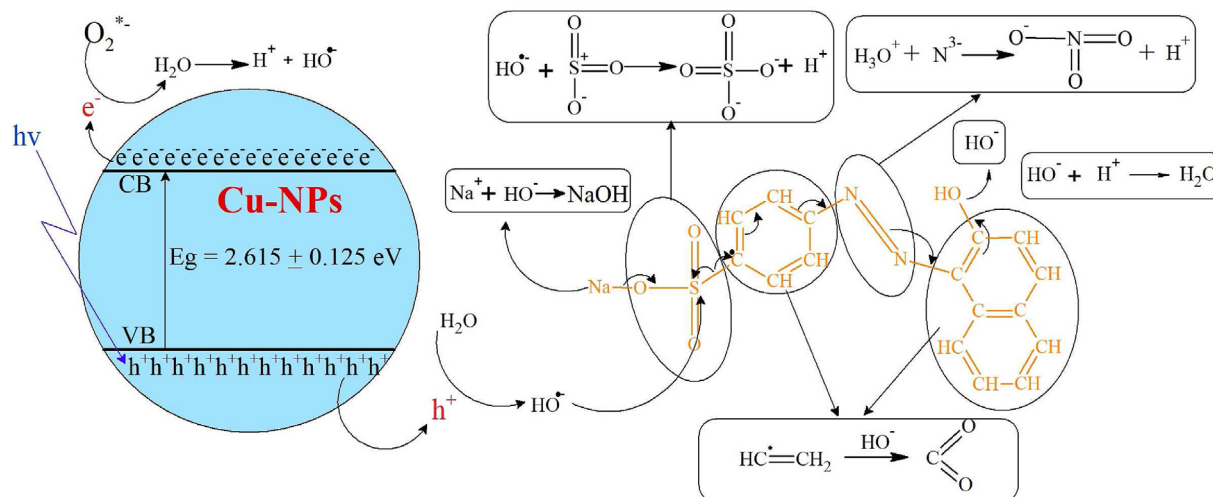
Table 3. Comparison of degradation efficiency with other nanoparticles.

Nanoparticles	Dyes	Dosage (mg)	Initial concentration of dyes (mg L^{-1})	Degradation efficiency (%)	Ref.
CuO	Methyl orange	0.015	30	97.18	[39]
CeO$_2$	Acid orange	0.01	10	95.4	[54]
Cu	Methylene blue	10	10	90	[42]
Mn0$_2$	Methyl orange	20	90	98.37	[59]
TiO$_2$	Methyl orange	6	50	93.97	[60]
Cu	Acid orange	0.05	50	81.07	present

4. Conclusion

The green synthesis process of Cu-NPs using red dragon fruit peel wasted extract and its photo-catalytic properties for the AO7 degradation process have been studied. Based on the FTIR analysis, it shows the presence of the phenolic or alcoholic groups in the extract, which plays an important role in the bio-reduction process. Furthermore, the characterization studies confirmed that the crystal structure of Cu-NPs was face-centered cubic (FCC) with an average crystallite size of 8.65−12.4 nm for all samples. The morphological parameter using SEM revealed that all samples have a spherical

shape and their monodispersed diameter size ranged from 10 to 80 nm. The green Cu-NPs produced a large surface area of 244.38—278.85 m^2g^{-1} and the calculated direct Eg value using Tauc's plot was 2.49—2.74 eV. These results indicated that the synthesized Cu-NPs have good properties as a photocatalyst on dye degradation of AO7. Under UV light, the product was used as a photocatalyst, and it showed a high degradation efficiency of 81.07% on organic dye AO7 with a reusability of 3—4 cycles. These results also revealed that there was a 20% decrease in degradation efficiency. The overall study showed that Cu-NPs were successfully synthesized using the green method and applied as a photocatalysts for AO7 dyes.

Acknowledgment

References

[1] S.E. Putri, A. Ahmad, I. Raya, R.T. Tjahjanto, R. Irfandi, Synthesis and antibacterial activity of chitosan nanoparticles from black tiger shrimp shell (Penaeus monodon), Egypt, J. Chem. (2022) 1—10, https://doi.org/10.21608/ejchem.2022.148340.6417.

[2] D.A. Aina, O. Owolo, A. Lateef, F.O. Aina, A.S. Hakeem, Biomedical applications of chasmanthera dependens stem extract mediated silver nanoparticles as antimicrobial, antioxidant, anticoagulant, thrombolytic, and larvicidal agents, Karbala Int. J. Mod. Sci. 5 (2019) 71—80, https://doi.org/10.33640/2405-609X.1018.

[3] Z. Sabouri, S. Sabouri, S.S.T.H. Moghaddas, A. Mostafapour, S.M. Gheibihayat, M. Darroudi, Plant-based synthesis of Ag-doped ZnO/MgO nanocomposites using Caccinia macranthera extract and evaluation of their photocatalytic activity, cytotoxicity, and potential application as a novel sensor for detection of Pb^{2+} ions, Biomass Convers. Biorefinery. 12 (2022) 1—13, https://doi.org/10.1007/s13399-022-02907-1.

[4] R. Sierra, M. Pérez, G. Cadenas, V. Comparán, C. Ávila, O. Camacho, E. Jiménez, E. Hernández, J. Rm, Synthesis of copper nanoparticles using mixture of allylamine and poly-allylamine, J. Nanomater. 201 (2015) 1—9, https://doi.org/10.1155/2015/367341.

[5] R.B. Galindo, P.Y.R. Rodriguez, B.A.P. Urbina, C.A.A. Orta, O.S.R. Fernandez, G.C. Pliego, R.H.L. Saldivar, L.A.G. Cerde, Synthesis of copper nanoparticles by thermal decomposition and their antimicrobial properties, J. Nanomater. 201 (2014) 1—5, https://doi.org/10.1155/2013/980545.

[6] S. Hossain, U.K. Fatema, M.Y.A. Mollah, M.M. Rahman, M.A. Bin Hasan susan, Microemulsions as nanoreactors for preparation of nanoparticles with antibacterial activity, J. Bangladesh Chem. Soc. 25 (2012) 71—79, https://doi.org/10.3329/jbcs.v25i1.11777.

[7] H. Tavakoli, R. Sarraf-Mamoory, A.R. Zarei, Solvothermal synthesis of copper nanoparticles loaded on multi-wall carbon nanotubes as catalyst for thermal decomposition of ammonium perchlorate, J. Adv. Mater. Process. 3 (2018) 3—10, https://doi.org/10.1155/2013/980324.

[8] N. Wongpisutpaisan, P. Charoonsuk, N. Vittayakorn, W. Pecharapa, Sonochemical synthesis and characterization of copper oxide nanoparticles, Energy Proc. 9 (2011) 404—409, https://doi.org/10.1016/j.egypro.2011.09.044.

[9] V.D. Kulkarni, P.S. Kulkarni, Green synthesis of copper nanoparticles using ocimum sanctum leaf extract, Int. J. Chem. Stud. 1 (2018) 2321—4902, https://doi.org/10.21608/ejchem.2022.148340.6417.

[10] J.J. Mohindru, U.K. Garg, Ijesrt international journal of engineering sciences & Research technology green synthesis of copper nanoparticles using tea leaf extract, Int. J. Eng. Sci. Res. Technol. 307 (2017) 307—311, https://doi.org/10.5281/zenodo.827502.

[11] M. Batoool, B. Masood, Green synthesis of copper nanoparticles using solanum lycopersicum (tomato aqueous extract) and study characterization, J. Nanosci. Nanotechnol. Res. 11 (2017) 1—4, https://doi.org/10.1080/10667857.2020.186259.

[12] Z. Sabouri, M. Sabouri, M.S. Amiri, M. Khatami, M. Darroudi, Plant-based synthesis of cerium oxide nanoparticles using Rheum turkestanicum extract and evaluation of their cytotoxicity and photocatalytic properties, Mater. Technol. 37 (2022) 555—568, https://doi.org/10.1080/10667857.2020.1863573.

[13] P. Tshireletso, C.N. Ateba, O.E. Fayemi, Spectroscopic and antibacterial properties of CuONPs from orange, lemon and tangerine peel extracts: potential for combating bacterial resistance, Molecules 26 (2021) 1—12, https://doi.org/10.3390/molecules26030586.

[14] K. Vishveshvar, M.V. Aravind Krishnan, K. Haribabu, S. Vishnuprasad, Green synthesis of copper oxide nanoparticles using ixiro coccinea plant leaves and its characterization, Bionanoscience 8 (2018) 554—558, https://doi.org/10.1007/s12668-018-0508-5.

[15] P. Kumari, P.K. Panda, E. Jha, N. Pramanik, K. Nisha, K. Kumari, N. Soni, M.A. Mallick, S.K. Verma, Molecular insight to in vitro biocompatibility of phytofabricated copper oxide nanoparticles with human embryonic kidney cells, Nanomedicine 13 (2018) 2415—2433, https://doi.org/10.2217/nnm-2018-0175.

[16] Z. Sabouri, S. Sabouri, S.S. Tabrizi Hafez Moghaddas, A. Mostafapour, M.S. Amiri, M. Darroudi, Facile green synthesis of Ag-doped ZnO/CaO nanocomposites with Caccinia macranthera seed extract and assessment of their cytotoxicity, antibacterial, and photocatalytic activity, Bioproc. Biosyst. Eng. 45 (2022) 1799—1809, https://doi.org/10.1007/s00449-022-02786-w.

[17] D.A.S. Dawood, L.S. Chua, T.S. Tan, A.F. Alshemary, Biosynthesis, characterization and antiproliferative activity of green synthesized gold nanoparticles using Lantadene A extracted from Lantana camara, Karbala Int. J. Mod. Sci. 7 (2021) 313—326, https://doi.org/10.33640/2405-609X.3158.

[18] N.A. Zakariya, W.H.W. Jusof, S. Majeed, Green approach for iron oxide nanoparticles synthesis: application in antimicrobial and anticancer- an updated review, Karbala Int. J. Mod. Sci. 8 (2022) 421—437, https://doi.org/10.33640/2405-609X.3256.

[19] H. Veisi, B. Karmakar, T. Tamoradi, S. Hemmati, M. Hekmati, M. Hamelian, Biosynthesis of CuO nanoparticles using aqueous extract of herbal tea (Stachys Lavandulifolia) flowers and evaluation of its catalytic activity, Sci. Rep. 11 (2021) 1—13, https://doi.org/10.1038/s41598-021-81320-6.

[20] L.C. Wu, H.W. Hsu, Y.C. Chen, C.C. Chiu, Y.I. Lin, J.A.A. Ho, Antioxidant and antiproliferative activities of red pitaya, Food Chem. 95 (2006) 319—327, https://doi.org/10.1016/j.foodchem.2005.01.002.

[21] I. Fidrianny, N. Ilham, R. Hartati, Antioxidant profile and phytochemical content of different parts of super red dragon fruit (Hylocereus costaricensis) collected from West Java-Indonesia, Asian J. Pharmaceut. Clin. Res. 10 (2017) 290—294, https://doi.org/10.22159/ajpcr.2017.v10i12.21571.

[22] T.E. Purbaningtias, A.C. Aprilia, L. Fauzi`ah, The study of temperature and UV light effect in anthocyanin extract from dragon fruit (Hylocereus costaricensis) rind using

UV-Visible spectrophotometer, AIP Conf. Proc. 1911 (2017) 1—6, https://doi.org/10.1063/1.5016007.

[23] N.S. Al-Radadi, Biogenic proficient synthesis of (Au-NPs) via aqueous extract of Red Dragon Pulp and seed oil: characterization, antioxidant, cytotoxic properties, anti-diabetic anti-inflammatory, anti-Alzheimer and their anti-proliferative potential against cancer cell, Saudi J. Biol. Sci. 29 (2022) 2836—2855, https://doi.org/10.1016/j.sjbs.2022.01.001.

[24] Z.I. Ali, O.A. Ghazy, G. Meligi, H.H. Saleh, M. Bekhit, Radiation-induced synthesis of copper/poly(vinyl alcohol) nanocomposites and their catalytic activity, Adv. Polym. Technol. 37 (2018) 365—375, https://doi.org/10.1002/adv.21675.

[25] A.M. El Sayed, S. El-Gamal, W.M. Morsi, G. Mohammed, Effect of PVA and copper oxide nanoparticles on the structural, optical, and electrical properties of carboxymethyl cellulose films, J. Mater. Sci. 50 (2015) 4717—4728, https://doi.org/10.1007/s10853-015-9023-z.

[26] T. Sinha, M. Ahmaruzzaman, Photocatalytic decomposition behavior and reaction pathways of organic compounds using Cu nanoparticles synthesized: via a green route, Photochem. Photobiol. Sci. 15 (2016) 1275—1281, https://doi.org/10.1039/c6pp00116e.

[27] P. Raizada, A. Sudhaik, S. Patial, V. Hasija, A.A. Parwaz Khan, P. Singh, S. Gautam, M. Kaur, V.H. Nguyen, Engineering nanostructures of CuO-based photocatalysts for water treatment: current progress and future challenges, Arab. J. Chem. 13 (2020) 8424—8457, https://doi.org/10.1016/j.arabjc.2020.06.031.

[28] T. Aftab, Sustainable Management of Environmental Contaminants, Springer Nature, Switzerland. 2022.

[29] Z. Sabouri, M. Sabouri, S.S.T.H. Moghaddas, M. Darroudi, Design and preparation of amino-functionalized core-shell magnetic nanoparticles for photocatalytic application and investigation of cytotoxicity effects, J. Environ. Heal. Sci. Eng. 39 (2022) 223—235, https://doi.org/10.1007/s40201-022-00842-x.

[30] S. Kader, M.R. Al-Mamun, M.B.K. Suhan, S.B. Shuchi, M.S. Islam, Enhanced photodegradation of methyl orange dye under UV irradiation using MoO_3 and Ag doped TiO_2 photocatalysts, Environ. Technol. Innov. 27 (2022) 102476—102491, https://doi.org/10.1016/j.eti.2022.102476.

[31] S.E. Putri, D.E. Pratiwi, R.T. Tjahjanto, I. Andi, A. Rahman, I. Wulan, S. Ramadani, A.N. Ramadhani, A. Fudholi, The renewable of low toxicity gelcasting porous ceramic as Fe_2O_3 catalyst support on phenol photodegradation, Int. J. of Design and Nat. 17 (2022) 503—511, https://doi.org/10.18280/ijdne.170403.

[32] G.V. Caroling, A.M. Ranjitham, P. Shanthi, Biosynthesis of copper nanoparticles using aqueous Phyllanthus embilica (gooseberry) extract- characterisation and study of antimicrobial effects, Int. J. Nanomater. Chem. 10 (2015) 53—63. https://link.springer.com/10.1007/978-3-031-08446-1.

[33] S. Rahmati, A. Abdullah, E. Momeny, O.L. Kang, Optimization studies on microwave assisted extraction of dragon fruit (Hylocereus polyrhizus) peel pectin using response surface methodology, Int. Food Res. J. 22 (2015) 233—239, https://doi.org/10.1002/0470011149.

[34] B.H. Stuart, Infrared Spectroscopy: Fundamentals and Applications, John Wiley & Sons, New Jersey. 2005.

[35] J.L. White, Interpretation of infrared spectra of soil minerals, Soil Sci. 112 (1971) 22—31, https://doi.org/10.1097/00010694-197107000-00005.

[36] J. Xiong, Y. Wang, Q. Xue, X. Wu, Synthesis of highly stable dispersions of nanosized copper particles using L-ascorbic acid, Green Chem. 13 (2011) 900—904, https://doi.org/10.1039/c0gc00772b.

[37] K.-H. Tseng, H.-C. Ke, H.-C. Ku, Parameters and properties for the preparation of Cu nanocolloids containing polyvinyl alcohol using the electrical spark discharge method, Nanomater. Nanotechnol. 11 (2021) 184—198, https://doi.org/10.1177/18479804211035190.

[38] G. Caroling, M.N. Priyadharshini, E. Vinodhini, A.M. Ranjitham, P. Shanthi, Biosynthesis of copper nanoparticles using aqueous guava extract— characterisation and study of antibacterial effects, Int. J. Pharm. Biol. Sci. 5 (2015) 25—43, https://doi.org/10.1080/10667857.2020.1863573.

[39] I. Khan, I. Khan, M. Usman, M. Imran, K. Saeed, Nanoclay-mediated photocatalytic activity enhancement of copper oxide nanoparticles for enhanced methyl orange photodegradation, J. Mater. Sci. Mater. Electron. 31 (2020) 8971—8985, https://doi.org/10.1007/s10854-020-03431-6.

[40] N. Rauf, S. Ilyas, H. Heryanto, R. Rahmat, A.N. Fahri, M.H. Rahmi, D. Tahir, The correlation between structural and optical properties of zinc hydroxide nanoparticle in supports photocatalytic performance, Opt. Mater. (Amst). 112 (2021) 110780—110791, https://doi.org/10.1016/j.optmat.2020.110780.

[41] M.H. Habibi, R. Kamrani, R. Mokhtari, Fabrication and characterization of copper nanoparticles using thermal reduction: the effect of nonionic surfactants on size and yield of nanoparticles, Microchim. Acta 171 (2010) 91—95, https://doi.org/10.1007/s00604-010-0413-2.

[42] S.C. Mali, A. Dhaka, C.K. Githala, R. Trivedi, Green synthesis of copper nanoparticles using Celastrus paniculatus Willd. leaf extract and their photocatalytic and antifungal properties, Biotechnol. Reports 27 (2020) 518—523, https://doi.org/10.1016/j.btre.2020.e00518.

[43] J. Rouquerol, C. Fairbridge, D. Everett, J. Haynes, N. Pernicone, J. Ramsay, K. Sing, K. Unger, Recommendations for the characterization of porous solids, Pure Appl. Chem. 66 (1994) 1739—1751, https://doi.org/10.1351/pac199466081739.

[44] K. Sing, Reporting physisorption data for gas/solid systems with special reference to the determination of surface area and porosity (Recommendations 1984), Pure Appl. Chem. 57 (1985) 603—618, https://doi.org/10.1351/pac198557040603.

[45] C. Bueno-Ferrer, S. Parres-Esclapez, D. Lozano-Castelló, A. Bueno-López, Relationship between surface area and crystal size of pure and doped cerium oxides, J. Rare Earths 28 (2010) 647—653, https://doi.org/10.1016/S1002-0721(09)60172-1.

[46] M. Solehudin, U. Sirimahachai, G.A.M. Ali, K.F. Chong, S. Wongnawa, One-pot synthesis of isotype heterojunction g-C3N4-MU photocatalyst for effective tetracycline hydrochloride antibiotic and reactive orange 16 dye removal, Adv. Powder Technol. 31 (2020) 1891—1902, https://doi.org/10.1016/j.apt.2020.02.020.

[47] M.J. Ndolomingo, R. Meijboom, Determination of the surface area and sizes of supported copper nanoparticles through organothiol adsorption, Appl. Surf. Sci. 390 (2016) 224—235, https://doi.org/10.1016/j.apsusc.2016.08.080.

[48] N.R. Dhineshbabu, V. Rajendran, N. Nithyavathy, R. Vetumperumal, Study of structural and optical properties of cupric oxide nanoparticles, Appl. Nanosci. 6 (2016) 933—939, https://doi.org/10.1007/s13204-015-0499-2.

[49] D.R.A. Preethi, A. Philominal, Green synthesis of pure and silver doped copper oxide nanoparticles using Moringa Oleifera leaf extract, Mater. Lett. X. 13 (2022) 100122—100139, https://doi.org/10.1016/j.mlblux.2022.100122.

[50] O. Access, Effect of pH Concentration on Facile Synthesized Copper 16 (2022) 54—58, https://doi.org/10.17756/nwj.2022-s1-011.

[51] R.S. Mohammed, Synthesis of CuO/ZnO and MgO/ZnO core/shell nanoparticles with plasma jets and study of their structural and optical properties, Karbala Int. J. Mod. Sci. 8 (2022) 213—222, https://doi.org/10.33640/2405-609X.3225.

[52] A. Naeimi, A. Sharifi, L. Montazerghaem, A.R. Abhari, Z. Mahmoodi, Z.H. Bakr, A.V. Soldatov, G.A.M. Ali, Transition metals doped WO_3 photocatalyst towards high efficiency decolourization of azo dye, J. Mol. Struct. 1250 (2022) 3—10, https://doi.org/10.1016/j.molstruc.2021.131800.

[53] B.S. Muthukrishnan S, S.M. Muthukumar M, S.K. T. Rao Mv, Catalytic degradation of organic dyes using synthesized

silver nanoparticles: a green approach, J. Biorem. Biodegrad. 16 (2015) 15—21, https://doi.org/10.4172/2155-6199.1000312.

[54] K. Hamidian, A. Najafidoust, A. Miri, M. Sarani, Photo-catalytic performance on degradation of Acid Orange 7 dye using biosynthesized un-doped and Co doped CeO_2 nano-particles, Mater. Res. Bull. 138 (2021) 111206—111219, https://doi.org/10.1016/j.materresbull.2021.111206.

[55] K. Elgendy, I. Elmehasseb, S. Kandil, Efficient removal of common organic pollutants from water by Zn-doped TiO2 nanoparticles with different applications, Karbala Int. J. Mod. Sci. 8 (2022) 223—236, https://doi.org/10.33640/2405-609X.3226.

[56] A.S. Ethiraj, P. Uttam, V.K.K.F. Chong, G.A.M. Ali, Photo-catalytic performance of a novel semiconductor nanocatalyst: copper doped nickel oxide for phenol degradation, Mater. Chem. Phys. 242 (2020) 122520—122532, https://doi.org/10.1016/j.matchemphys.2019.122520.

[57] L. Hua, H. Ma, L. Zhang, Degradation process analysis of the azo dyes by catalytic wet air oxidation with catalyst CuO/γ-

Al_2O_3, Chemosphere 90 (2013) 143—149, https://doi.org/10.1016/j.chemosphere.2012.06.018.

[58] A. Sharma, R.K. Dutta, Studies on the drastic improvement of photocatalytic degradation of acid orange-74 dye by TPPO capped CuO nanoparticles in tandem with suitable electron capturing agents, RSC Adv. 5 (2015) 43815—43823, https://doi.org/10.1039/c5ra04179a.

[59] X. Zhang, B. Zhou, S. Yin, Y. Wang, X. Zhang, Q. Meng, F. Meng, C. Wei, G. Wen, Mesoporous manganese dioxide prepared by nano-casting: an efficient catalyst for of methyl orange and oxalic acid degradation in aqueous solution, Vacuum 206 (2022) 111495—111511, https://doi.org/10.1016/j.vacuum.2022.111495.

[60] M. Pirsaheb, H. Hossaini, S. Nasseri, N. Azizi, B. Shahmoradi, T. Khosravi, Optimization of photocatalytic degradation of methyl orange using immobilized scoria-Ni/ TiO_2 nanoparticles, J. Nanostructure Chem. 10 (2020) 143—159, https://doi.org/10.1007/s40097-020-00337-x.